Sensors and Materials, Vol. 35, No. 2 (2023) 439–449
MYU Tokyo

S & M 3180

Ionizing-radiation-induced Scintillation Characteristics of Ti-doped $SrZrO_3$ Single Crystal

Daiki Shiratori,* Hiroyuki Fukushima, Daisuke Nakauchi, Takumi Kato, Noriaki Kawaguchi, and Takayuki Yanagida

Nara Institute of Science and Technology,
8916-5 Takayama, Ikoma, Nara 630-0192, Japan

(Received October 1, 2022; accepted January 12, 2023)

Keywords: scintillation, $SrZrO_3$ single crystal, photoluminescence, perovskite

In this study, $SrZrO_3$ single crystals doped with 0, 0.3, 1.0, and 3.0% Ti were successfully synthesized by the floating zone method, and their optical and scintillation properties were investigated. Both the photoluminescence (PL) and scintillation spectra revealed a broad emission band centered at 400 nm, and the decay time constants were of μs order. All the Ti-doped specimens exhibited clear full energy peaks under ^{241}Am α-ray irradiation. The obtained PL quantum yield and pulse height spectra suggest that the optimum Ti concentration among our specimens is 3.0%.

1. Introduction

Scintillators instantaneously convert high-energy photons of ionizing radiation to lower-energy photons and are used in photodetectors, such as photomultiplier tubes (PMTs), to detect radiation. The applications of scintillators are very wide, for example, medical diagnosis,[1–4] high-energy and nuclear physics,[5–7] security,[8,9] and personal dose monitoring.[10–12] Thus, users must select appropriate scintillators depending on the application. In addition, when detecting ionizing radiation, different scintillators are used for different radiation species. In particular, for X-rays and γ-rays, it is important that the scintillators consist of heavy elements and have high density.

In recent years, single crystals with Hf have been attracting attention as potential new scintillators because of their relatively high density.[13,14] The detection efficiency for X-rays and γ-rays depends on the density and effective atomic number of the scintillators. Therefore, these materials are potential scintillators for detecting high-energy ionizing radiation. However, the single-crystal growth of these materials, which have a high melting point, by the Czochralski and Bridgman–Stockbarger methods is difficult, since these methods require a crucible. To grow these high-melting-point materials, a crucible-free growth method such as the floating zone (FZ) method can be used.[15] Our group has successfully synthesized some high-melting-point single crystals, for example,

*Corresponding author: e-mail: shiratori.daiki.sc3@ms.naist.jp
https://doi.org/10.18494/SAM4140

ISSN 0914-4935
https://myukk.org/

$CaHfO_3$[16,17] and $RE_2Hf_2O_7$ (*RE* = La, Gd, and Lu)[14,18] doped with Ce and Ti. In particular, perovskite-type $CaHfO_3$ crystals exhibited the best scintillation properties among the Hf compounds we examined. On the basis of these results, we have also focused on compounds of Zr, which is a homologous element to Hf. $MZrO_3$ (*M* = Ca, Sr) has the same structure as $CaHfO_3$, and $SrZrO_3$ also has a relatively high density of ~5.5 g/cm^3.[19] In addition, Zr oxides have high melting points and are suitable for applying the FZ method. The scintillation properties of Ce- and Ti-doped $CaZrO_3$ single crystals have been investigated.[20,21] Ti-doped $CaZrO_3$ clearly showed photoabsorption peaks under ^{137}Cs γ-ray irradiation. In this study, we focused on $SrZrO_3$, which has the same perovskite structure as $CaZrO_3$, with the aim of increasing the interaction efficiency with ionizing radiation and improving the scintillation properties of the system. Luminescence related to Ti^{4+} appears at around 400–500 nm because luminescence centers are affected by the crystal symmetry and structure. The quantum efficiency of PMTs depends on the emission wavelength, and bluish luminescence is suitable for common PMTs. In addition, the decay time constant is approximately of μs order in some materials, making them applicable for photon-counting measurement. Therefore, we selected Ti as a luminescent center.

2. Materials and Methods

2.1 Preparation method

All specimens were synthesized using the FZ method. First, raw powders of SrO (99.99%, FUJIFILM Wako Pure Chemical Corporation), ZrO_2 (99.99%, Furuuchi Chemical Corporation), and TiO_2 (99.99%, Kojundo Chemical Laboratory Co., Ltd.) were mixed with stoichiometric ratios. Then, the homogeneously mixed powder was formed into a cylindrical rod by applying hydrostatic pressure to the mixture loaded in a cylindrical balloon. Finally, the obtained rod was sintered in the atmosphere to obtain a solid ceramic rod in three steps: at 1100 °C for 8 h, 1250 °C for 8 h, and 1500 °C for 8 h. The crystal growth was performed using an optical FZ furnace equipped with four 3 kW xenon arc lamps (Crystal Systems FZ-T-12000-X-VPO-PC-YH) and four ellipsoidal mirrors having a vertically positioned optical axis, which provided axially symmetric heating of the zone. The sintered rod was loaded into the FZ furnace, and the crystal growth was conducted with a pull-down rate of 30 mm/h and a rotation rate of 20 rpm. The as-synthesized crystals were cut into specimens of ⌀3–4 × ~1 mm^3, whose surfaces were optically polished.

2.2 Analysis method

X-ray diffraction (XRD) patterns were measured using a MiniFlex 600 diffractometer (Rigaku). We measured the optical properties of the specimens to determine the origin of their luminescence. A Quantaurus-QY system (C11347, Hamamatsu Photonics) was used to evaluate the photoluminescence (PL) excitation/emission contour maps and PL quantum yields (*QY*s).

The excitation and emission wavelength ranges used in monitoring were 250–400 and 300–650 nm, respectively, with 10 nm intervals. PL lifetime measurements were performed using a Quantaurus-Tau PL lifetime measurement system (C11367, Hamamatsu Photonics).

We measured scintillation spectra using our laboratory-made setup.[22] We used an X-ray generator (XRB80N100/CB, Spellman) equipped with a conventional X-ray tube as the X-ray source. The operation current and tube voltage of the X-ray tube were 1.2 mA and 40 kV, respectively. The scintillation obtained by X-ray irradiation was guided through an optical fiber to a Shamrock 163 monochromator equipped with an Andor DU-420-BU2 CCD-based detector. Scintillation lifetime and afterglow profiles were measured using a Hamamatsu Photonics custom-made system.[23] The light yield is an important parameter that determines the efficiency of the scintillating material in actual device applications. Light yields were evaluated from pulse height spectra under ^{241}Am 5.4 MeV α-ray irradiation using our original setup.[24] The specimens were optically coupled with a PMT (R7600, Hamamatsu) using optical grease (TSK5353, OKEN). The signal generated from the PMT was fed into an ORTEC 113 pre-amplifier, an ORTEC 570 shaping amplifier, and Amptec 8000A multichannel analyzer (8000A, Amptec), and finally a PC.

3. Results and Discussion

Figure 1 shows a photograph of the synthesized undoped and Ti-doped specimens under LED light. The crystal specimens are colorless and transparent to the naked eye. In the 1.0 and 3.0% Ti-doped specimens, cloudiness can be observed in part of the crystals. Since the XRD pattern discussed below shows only a single $SrZrO_3$ phase, it is considered that a polycrystalline phase was partially generated. Figure 2 shows the powder XRD patterns of all the specimens. The XRD patterns were in good agreement with the standard pattern of $SrZrO_3$, indicating only single-phase $SrZrO_3$ with the *Pnma* space group of the orthorhombic crystal system [Fig. 2(a)].[25] Furthermore, the diffraction peaks slightly shifted toward a higher angle with increasing Ti concentration in the crystals, because the ionic radius of Zr^{4+} (0.72 Å) is higher than that of its Ti^{4+} (0.61 Å) counterpart [Fig. 2(b)].[26]

PL 3D contour maps of the undoped and Ti-doped specimens are shown in Fig. 3. When the specimens were excited with 280–300 nm UV light, a broad emission band at around 400 nm

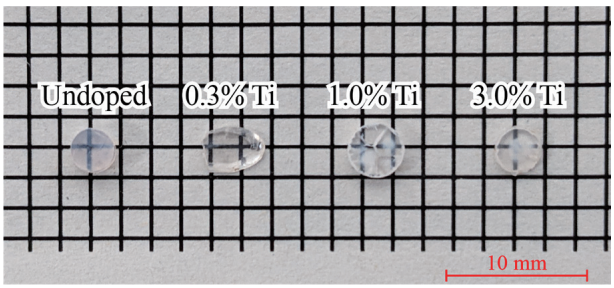

Fig. 1. (Color online) Photograph of undoped and Ti-doped specimens under LED light.

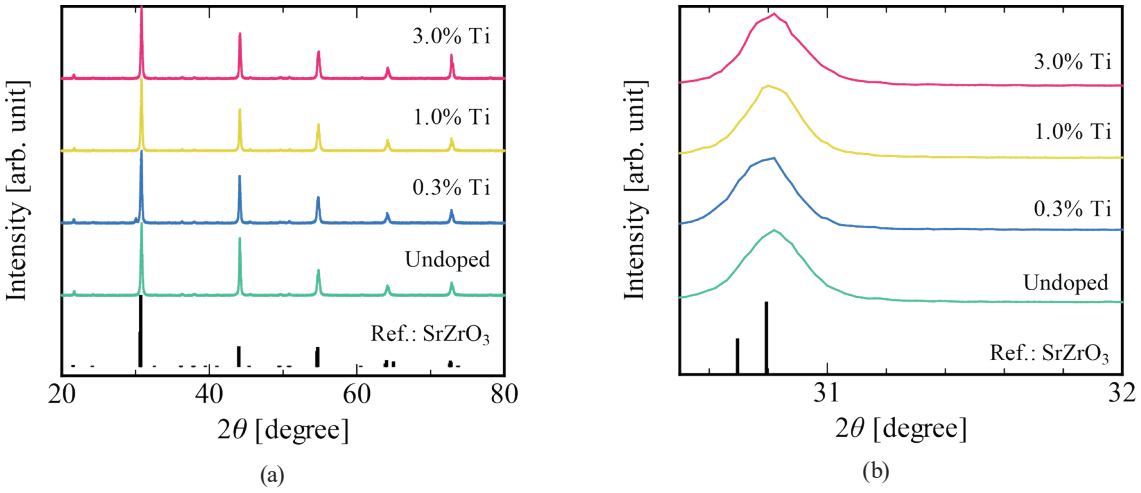

Fig. 2. (Color online) (a) XRD patterns of undoped and Ti-doped specimens and (b) enlarged figure around 30°.

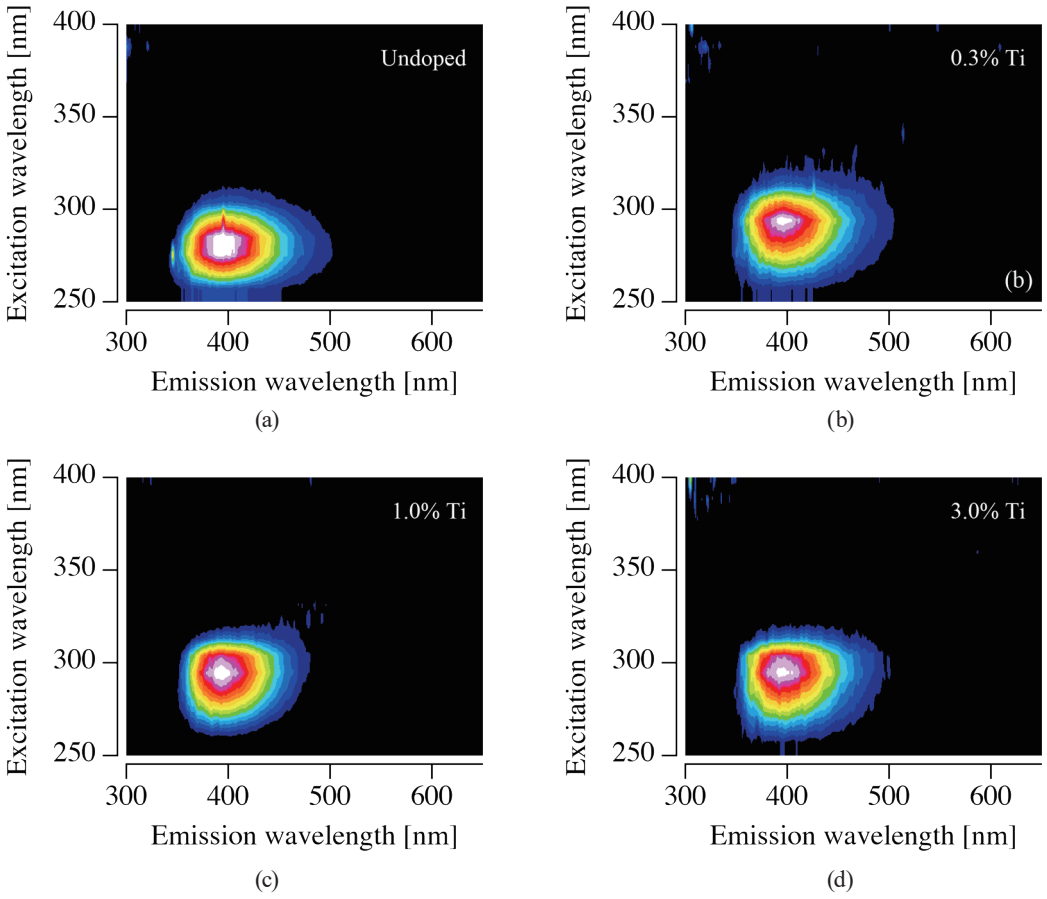

Fig. 3. (Color online) PL contour maps of (a) undoped, (b) 0.3% Ti-doped, (c) 1.0% Ti-doped, and (d) 3.0% Ti-doped specimens.

was observed in all specimens. In addition, the observed spectral features of the emissions were similar for all specimens, but the excitation band shifted to a longer wavelength with increasing Ti concentration. To determine the origin of these emissions, the PL lifetime was measured. Figure 4 shows the PL decay time profiles of the undoped and Ti-doped specimens, where the excitation and monitoring wavelengths were 280 and 400 nm, respectively. The obtained PL decay curves were approximated by the single exponential decay function $I = A\exp(-t/\tau)$, where I and A are the signal intensity at times t and 0, respectively, and τ is the PL lifetime. The calculated PL lifetimes are shown in Table 1. They were in agreement with those of some Ti-doped phosphors in a previous study. The lifetime of the Ti-related emission appears to depend on the matrix crystal, but mostly previously reported lifetimes were of μs order.[14,16,20,27] Therefore, considering the emission wavelength and PL lifetime, we attributed the emissions at around 400 nm to charge-transfer (CT) transitions of Ti^{4+}–O^{2-}.[27,28] CT emission generally follows a spin- and dipole-allowed absorption. In this case, the promotion of an electron from nonbonding orbitals (ground state) to antibonding orbitals (excited state) in one complex occurs, resulting in a marked distortion of the excited state relative to the ground state; therefore, the

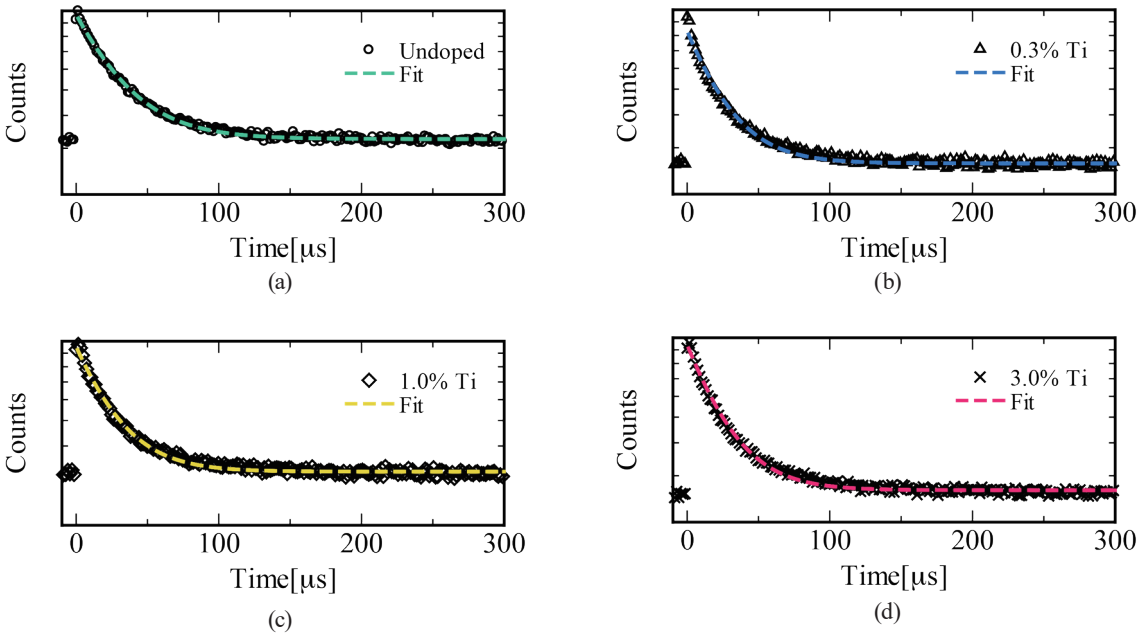

Fig. 4. (Color online) PL decay curves of (a) undoped, (b) 0.3% Ti-doped, (c) 1.0% Ti-doped, and (d) 3.0% Ti-doped specimens.

Table 1
PL *QY*, PL lifetimes, and kinetics of undoped and Ti-doped specimens.

Ti concentration	*QY* (%)	PL lifetime (μs)	k_r (s^{-1})	k_{nr} (s^{-1})
Undoped	14.8	29.4	5.0×10^3	2.89×10^4
0.3%	18.6	23.6	7.8×10^3	3.44×10^4
1.0%	16.1	24.4	6.6×10^3	3.43×10^4
3.0%	18.2	23.6	7.7×10^3	3.46×10^4

spectral bands become broad.[29] A broad excitation spectrum can also be observed in Ti-related CT emission, which includes multiple excitation bands. Furthermore, it has been reported that the intensity ratio of its excitation bands changes with increasing Ti concentration.[30] On the basis of this fact, the redshift of the excitation band with increasing Ti doping is attributed to a newly appearing excitation band at ~300 nm associated with CT emission. Table 1 lists the observed PL *QY* of each specimen for 400 nm emission. The 0.3% Ti-doped specimen showed the highest PL *QY* of 18.6% among the specimens, and the PL *QY* value was uncorrelated with the Ti concentration. The highest PL *QY* value was approximately three times that of the Ti-doped $CaZrO_3$ single crystal grown by the FZ method.[20] The Ti-related emission was observed even in the undoped specimen, which was due to the presence of a small amount of Ti in the ZrO_2 raw powder. To further consider the relationship between the PL characteristics and Ti concentration, we calculated the radiative transition rate denoted as k_r. The observed PL lifetime τ can be expressed by $\tau = 1/(k_r + k_{nr})$, where the k_{nr} is the non-radiative transition rate. In addition, the PL *QY* is expressed as $QY = k_r/(k_r + k_{nr})$. From these relationships, the transition rate can be obtained as

$$k_r = QY/\tau, \tag{1}$$

$$k_{nr} = (1 - QY)/\tau. \tag{2}$$

The calculated kinetics k_r and k_{nr} for each specimen are also summarized in Table 1. The k_r values are consistent with the tendency for the PL *QY* to increase or decrease in these emissions, suggesting the validity of the respective PL lifetimes. On the other hand, k_{nr} was lowest in the undoped specimen and almost equal to that in the Ti-doped specimens.

Figure 5 shows the scintillation spectra of the Ti-doped specimens under X-ray irradiation. A broad emission band centered at 400 nm appeared in all the Ti-doped specimens. All specimens exhibited the band also observed in the PL spectra; the undoped sample had an additional band

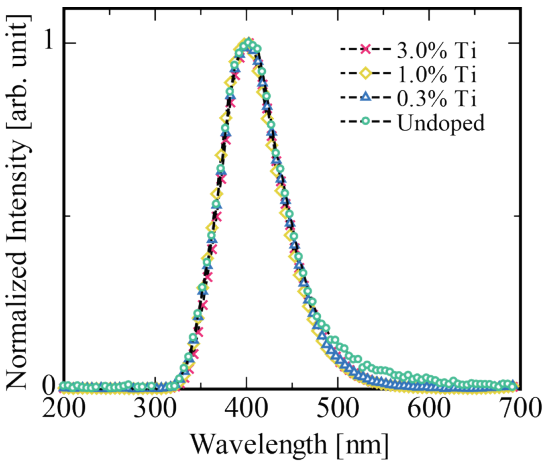

Fig. 5. (Color online) X-ray-induced scintillation spectra of undoped and Ti-doped specimens.

at a longer wavelength. This feature is also observed in Ti-doped specimens, and the result is explained by the presence of two origins of the luminescence. Figure 6 shows the X-ray-induced scintillation decay curves of the undoped and Ti-doped specimens. The measured decay curves were approximated by three exponential functions, and the scintillations lifetimes were calculated, which are listed in Table 2. The fast component τ_1 is assumed to be due to instrumental response functions. On the other hand, τ_3 is reasonable as the μs-order lifetime observed in the PL, which appears to be the scintillation lifetime corresponding to the CT transition of Ti^{4+}–O^{2-}. τ_2 appears to correspond to the emission of the aforementioned longer-wavelength component, which is presumably due to some defect emission. According to previous studies on defect luminescence in $SrZrO_3$ crystals, luminescence due to oxygen vacancy defects (singly ionized $[ZrO_5 \cdot V_O^{\cdot}]$ complex state and doubly ionized $[ZrO_5 \cdot V_O^{\cdot\cdot}]$ complex state) are observed in the range of 500–600 nm.[31,32] Since the lifetime of the defect emission also approximately corresponds to the τ_2 values, it is reasonable to conclude that the emissions at around 500–600 nm are these defect emissions.

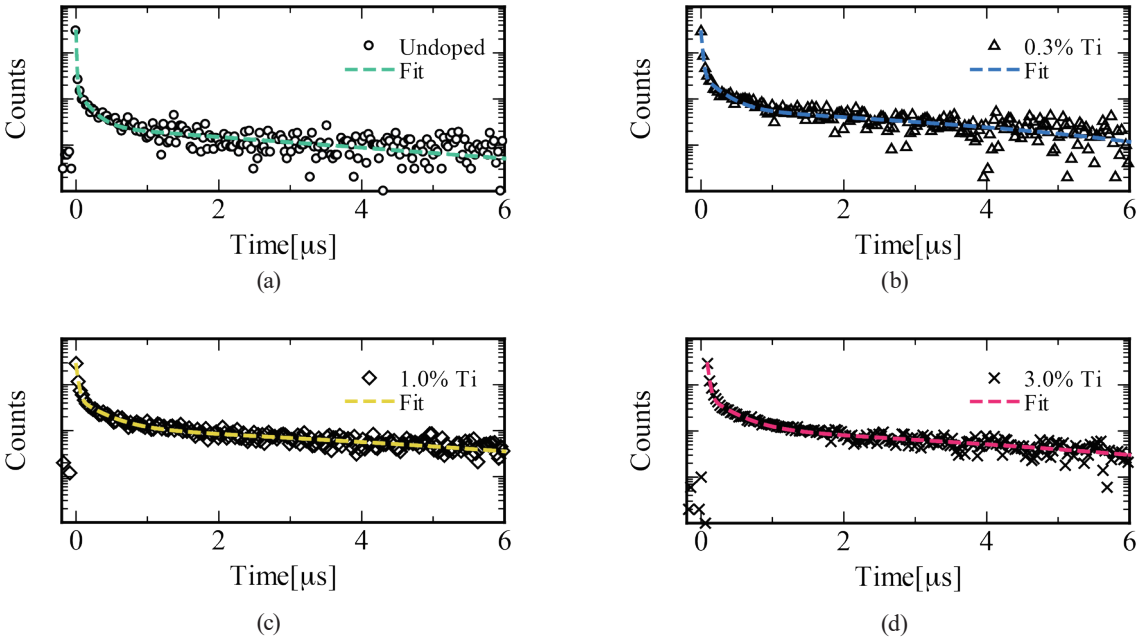

Fig. 6. (Color online) X-ray-induced scintillation decay curves of (a) undoped, (b) 0.3% Ti-doped, (c) 1.0% Ti-doped, and (d) 3.0% Ti-doped specimens.

Table 2
Scintillation lifetimes of undoped and Ti-doped specimens.

Ti concentration	Scintillation lifetime		
	τ_1 (ns)	τ_2 (ns)	τ_3 (ns)
Undoped	7.4	169	3.73
0.3%	10.1	138	13.0
1.0%	28.8	343	8.18
3.0%	28.0	336	6.95

Figure 7 shows the pulse height spectra of the undoped and Ti-doped specimens. All specimens showed a full energy peak when irradiated with α-rays from ^{241}Am. To determine the peak position of each specimen, we used the Gaussian function for fitting analysis. The calculated peak positions are shown in Table 3. The light yields (*LY*s) of the specimens were estimated relative to the light yield of the commercial glass scintillator GS20 ($4Ce_2O_3$–$18Li_2O$–$18Al_2O_3$–$4MgO$–$56SiO_2$ wt.%). The calculated values are also summarized in Table 3. The 3.0% Ti-doped specimen had the highest *LY* of approximately 12% of that of the GS20 counterpart. The *LY* values were simply positively correlated with the Ti concentration of the specimens and independent of the PL *QY*. Here, in the conventional Robbins model, the scintillation *LY* is proportional to a product of energy transfer efficiency from the host lattice to localized emission centers and PL *QY*.[33] Based on the model, the increase in *LY* was caused by the increase in the probability of secondary electrons generated by ionizing radiation reaching the luminescent centers because of the increase in Ti concentration in the host crystal.

Figure 8 shows the afterglow decay curves of the undoped and Ti-doped specimens, and the afterglow level (*Af*) of each specimen is summarized in Table 3. *Af* was evaluated as $Af = (I_{20} - I_{bg})/(I_m - I_{bg}) \times 100$, where I_m and I_{20} are the signal intensities under X-ray irradiation and 20 ms

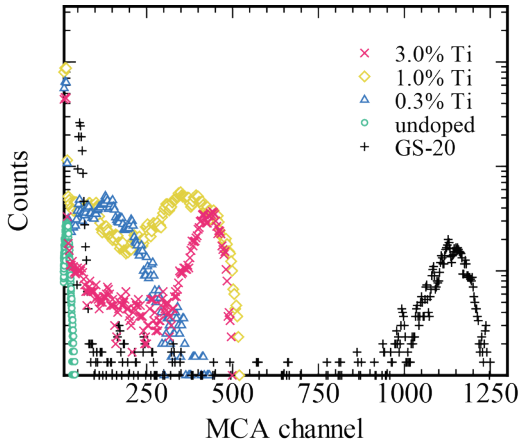

Fig. 7. (Color online) Pulse height spectra of undoped and Ti-doped specimens and GS20 scintillator under ^{241}Am α-ray irradiation.

Table 3
Scintillation *LY* values, experimental parameters in pulse height measurement, and *Af* values of undoped and Ti-doped specimens.

Ti concentration /Reference	Peak position	Gain	PMT voltage (V)	*LY* (ph/5.5 MeV)	*Af* (%)
Undoped	200	25	600	40	0.91
0.3%	130	2.5	700	270	2.07
1.0%	380	2.5	700	790	1.15
3.0%	430	2.5	700	890	0.96
GS20	1138	1	700	6900	N/A

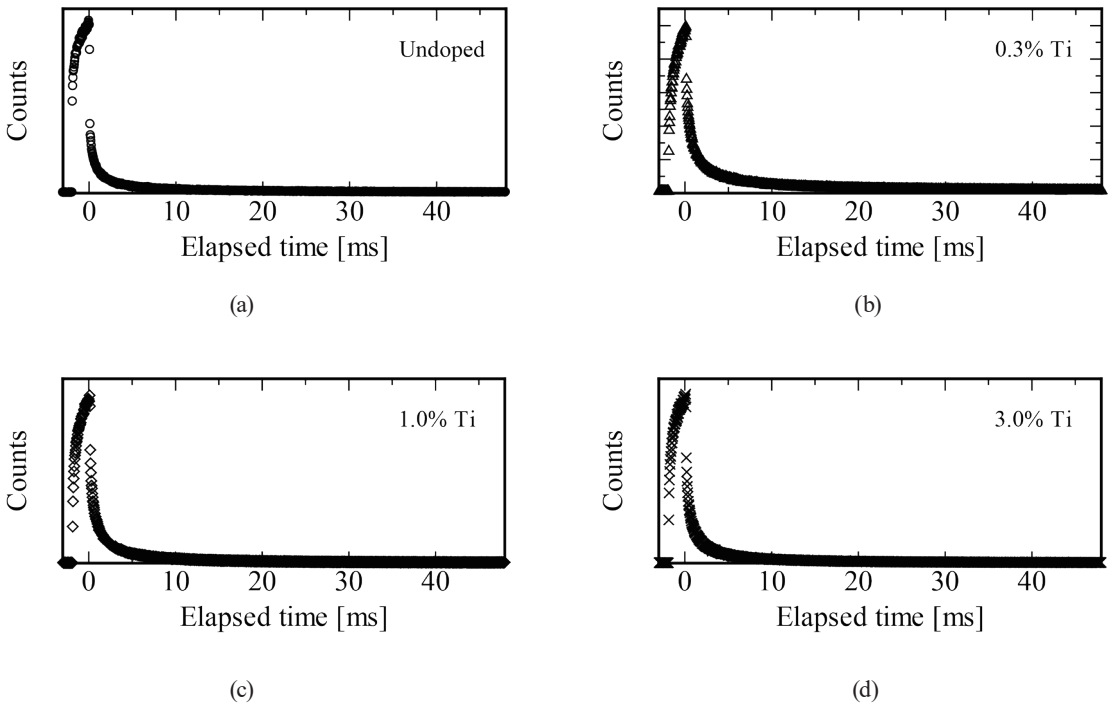

Fig. 8. (Color online) Afterglow decay curves of (a) undoped, (b) 0.3% Ti-doped, (c) 1.0% Ti-doped, and (d) 3.0% Ti-doped specimens.

after the end of X-ray irradiation, respectively. I_{bg} is the background level. The afterglow levels of the specimens are ~1% or more and decreased with increasing Ti concentration. $SrZrO_3$ single crystal has a strong afterglow compared with conventional scintillators.[23] Furthermore, the addition of Ti appears to induce more afterglow.

4. Conclusions

$SrZrO_3$ single crystals doped with 0, 0.3, 1.0, and 3.0% Ti were successfully synthesized by the FZ method and their optical and scintillation properties were investigated. Both the PL and scintillation spectra revealed a broad emission band centered at 400 nm, and the decay time constants were of μs order. All Ti-doped specimens exhibited clear full energy peaks under ^{241}Am α-ray irradiation. The obtained PL *QY* and pulse height spectra suggest that the optimum Ti concentration among our specimens is 3.0%.

Acknowledgments

This work was supported by Grants-in-Aid for Scientific Research A (22H00309), Scientific Research B (22H02939, 21H03733, and 21H03736), Exploratory Research (22K18997), and JSPS Fellows (20J23225) from the Japan Society for the Promotion of Science. The Cooperative Research Project of the Research Center for Biomedical Engineering is also acknowledged.

References

1 S. Basu, T. C. Kwee, S. Surti, E. A. Akin, D. Yoo, and A. Alavi: Ann. N. Y. Acad. Sci. **1228** (2011) 1. https://doi.org/10.1111/j.1749-6632.2011.06077.x.
2 W. W. Moses: Nucl. Instrum. Meth. A **471** (2001) 209. https://doi.org/10.1016/S0168-9002(01)00969-X.
3 P. Lecoq: Nucl. Instrum. Meth. A **809** (2016) 130. https://doi.org/10.1016/j.nima.2015.08.041.
4 P. Moskal, N. Zoń, T. Bednarski, P. Białas, E. Czerwiński, A. Gajos, D. Kamińska, Ł. Kapłon, A. Kochanowski, G. Korcyl, J. Kowal, P. Kowalski, T. Kozik, W. Krzemień, E. Kubicz, S. Niedźwiecki, M. Pałka, L. Raczyński, Z. Rudy, O. Rundel, P. Salabura, N. G. Sharma, M. Silarski, A. Słomski, J. Smyrski, A. Strzelecki, A. Wieczorek, W. Wiślicki, and M. Zieliński: Nucl. Instrum. Meth. A **775** (2015) 54. https://doi.org/10.1016/j.nima.2014.12.005.
5 I. Ogawa, R. Hazama, H. Miyawaki, S. Shiomi, N. Suzuki, Y. Ishikawa, G. Kunitomi, Y. Tanaka, M. Itamura, K. Matsuoka, S. Ajimura, T. Kishimoto, H. Ejiri, N. Kudomi, K. Kume, H. Ohsumi, and K. Fushimi: Nucl. Phys. A **730** (2004) 215. https://doi.org/10.1016/j.nuclphysa.2003.10.015.
6 N. J. C. Spooner, G. J. Davies, J. D. Davies, G. J. Pyle, T. D. Bucknell, G. T. A. Squier, J. D. Lewin, and P. F. Smith: Phys. Lett. B **321** (1994) 156. https://doi.org/10.1016/0370-2693(94)90343-3.
7 H. Abramowicz, J. G. H. de Groot, J. Knobloch, J. May, P. Palazzi, A. Para, F. Ranjard, J. Rothberg, W. von Rüden, W. D. Schlatter, J. Steinberger, H. Taureg, H. Wahl, J. Wotschack, F. Eisele, H. P. Klasen, K. Kleinknecht, B. Pszola, B. Renk, H. J. Willutzki, F. Dydak, T. Flottmann, C. Geweniger, J. Królikowski, K. Tittel, C. Guyot, J. P. Merlo, B. Peyaud, J. Rander, J. P. Schuller, R. Turlay, J. T. He, T. Z. Ruan, and W. M. Wu: Nucl. Instrum. Methods **180** (1981) 429. https://doi.org/10.1016/0029-554X(81)90083-5.
8 L. E. Sinclair, D. S. Hanna, A. M. L. MacLeod, and P. R. B. Saull: IEEE Trans. Nucl. Sci. **56** (2009) 1262. https://doi.org/10.1109/TNS.2009.2019271.
9 V. D. Ryzhikov, A. D. Opolonin, P. V. Pashko, V. M. Svishch, V. G. Volkov, E. K. Lysetskaya, D. N. Kozin, and C. Smith: Nucl. Instrum. Meth. A **537** (2005) 424. https://doi.org/10.1016/j.nima.2004.08.056.
10 S. W. S. McKeever: Nucl. Instrum. Meth. B **184** (2001) 29. https://doi.org/10.1016/S0168-583X(01)00588-2.
11 R. Yokota and H. Imagawa: J. Phys. Soc. Jpn. **23** (1967) 1038. https://doi.org/10.1143/JPSJ.23.1038.
12 C. C. Gronchi, S. G. P. Cecatti, T. C. N. O. Pinto, and L. V. E. Caldas: Nucl. Instrum. Meth. B **266** (2008) 2915. https://doi.org/10.1016/j.nimb.2008.03.139.
13 A. Grezer, E. Zych, and L. Kępiński: Radiat. Meas. **45** (2010) 386. https://doi.org/10.1016/j.radmeas.2009.09.014.
14 D. Nakauchi, T. Kato, N. Kawaguchi, and T. Yanagida: Sens. Mater. **32** (2020) 1389. https://doi.org/10.18494/SAM.2020.2751.
15 T. Akashi, K. Matumi, T. Okada, and T. Mizutani: IEEE Trans. Magn. **5** (1969) 285. https://doi.org/10.1109/TMAG.1969.1066457.
16 H. Fukushima, D. Nakauchi, N. Kawaguchi, and T. Yanagida: Jpn. J. Appl. Phys. **58** (2019) 052005. https://doi.org/10.7567/1347-4065/ab116c.
17 H. Fukushima, D. Nakauchi, G. Okada, N. Kawaguchi, and T. Yanagida: J. Mater. Sci.: Mater. Electron. **29** (2018) 21033. https://doi.org/10.1007/s10854-018-0249-9.
18 D. Nakauchi, G. Okada, N. Kawaguchi, and T. Yanagida: Jpn. J. Appl. Phys. **57** (2018) 100307. https://doi.org/10.7567/JJAP.57.100307.
19 A. Thongtha and T. Bongkarn: Key Eng. Mater. **421**–**422** (2009) 223. https://doi.org/10.4028/www.scientific.net/KEM.421-422.223.
20 H. Fukushima, D. Nakauchi, T. Kato, N. Kawaguchi, and T. Yanagida: Jpn. J. Appl. Phys. **61** (2022) SB1039. https://doi.org/10.35848/1347-4065/ac18a8.
21 H. Fukushima, D. Nakauchi, M. Koshimizu, N. Kawaguchi, and T. Yanagida: Jpn. J. Appl. Phys. **59** (2020) SCCB15. https://doi.org/10.7567/1347-4065/ab4a86.
22 T. Yanagida, K. Kamada, Y. Fujimoto, H. Yagi, and T. Yanagitani: Opt. Mater. **35** (2013) 2480. https://doi.org/10.1016/j.optmat.2013.07.002.
23 T. Yanagida, Y. Fujimoto, T. Ito, K. Uchiyama, and K. Mori: Appl. Phys. Express **7** (2014) 062401. https://doi.org/10.7567/APEX.7.062401.
24 D. Nakauchi, N. Kawaguchi, and T. Yanagida: Sens. Mater. **31** (2019) 1249. https://doi.org/10.18494/SAM.2019.2184.
25 V. M. Longo, L. S. Cavalcante, M. G. S. Costa, M. L. Moreira, A. T. de Figueiredo, J. Andrés, J. A. Varela, and E. Longo: Theor. Chem. Acc. **124** (2009) 385. https://doi.org/10.1007/s00214-009-0628-7.
26 J. Bera and S. K. Rout: Mater. Res. Bull. **40** (2005) 1187. https://doi.org/10.1016/j.materresbull.2005.03.029.
27 S. A. Basun, T. Danger, A. A. Kaplyanskii, D. S. McClure, K. Petermann, and W. C. Wong: Phys. Rev. B **54** (1996) 6141. https://doi.org/10.1103/PhysRevB.54.6141.

28 Y. Takebuchi, H. Fukushima, T. Kato, D. Nakauchi, N. Kawaguchi, and T. Yanagida: Radiat. Phys. Chem. **177** (2020) 109163. https://doi.org/10.1016/j.radphyschem.2020.109163.
29 G. Blasse and B. C. Grabmaier: Luminescent Materials (Springer Berlin Heidelberg, Berlin, Heidelberg, 1994), https://doi.org/10.1007/978-3-642-79017-1.
30 G.-H. Pan, L. Zhang, H. Wu, X. Qu, H. Wu, Z. Hao, L. Zhang, X. Zhang, and J. Zhang: J. Mater. Chem. C **8** (2020) 4518. https://doi.org/10.1039/C9TC06992E.
31 V. M. Longo, L. S. Cavalcante, R. Erlo, V. R. Mastelaro, A. T. de Figueiredo, J. R. Sambrano, S. de Lázaro, A. Z. Freitas, L. Gomes, N. D. Vieira, J. A. Varela, and E. Longo: Acta Mater. **56** (2008) 2191. https://doi.org/10.1016/j.actamat.2007.12.059.
32 S. K. Gupta, P. S. Ghosh, N. Pathak, A. Arya, and V. Natarajan: RSC Adv. **4** (2014) 29202. https://doi.org/10.1039/C4RA04262J.
33 D. J. Robbins: J. Electrochem. Soc. **127** (1980) 2694. https://doi.org/10.1149/1.2129574.